Information Flow in Planar Polarity

Katherine H Fisher[1], Alexander G Fletcher[2,3,*], David Strutt[1,4,*]

[1] Department of Biomedical Science, Firth Court, University of Sheffield, S10 2TN, UK

[2] School of Mathematics and Statistics, Hicks Building, University of Sheffield, S3 7RH, UK

[3] Bateson Centre, Firth Court, University of Sheffield, S10 2TN, UK

[4] Lead Contact

*Correspondence: a.g.fletcher@sheffield.ac.uk and d.strutt@sheffield.ac.uk

Keywords

Planar polarity, planar cell polarity, signalling, pattern formation, computational modelling, *Drosophila*

Summary

In developing tissues, sheets of cells become planar polarised, enabling coordination of cell behaviours. It has been suggested that ‘signalling’ of polarity information between cells may occur either bidirectionally or monodirectionally between the molecules Frizzled (Fz) and Van Gogh (Vang). Using computational modelling we find that both bidirectional and monodirectional signalling models reproduce known non-autonomous phenotypes derived from patches of mutant tissue of key molecules, but predict different phenotypes from double mutant tissue, which have previously given conflicting experimental results. Consequently, we re-examine experimental phenotypes in the *Drosophila* wing, concluding that signalling is most likely bidirectional. Our modelling suggests that bidirectional signalling can be mediated either *indirectly* via bidirectional feedbacks between asymmetric intercellular protein complexes, or *directly* via different affinities for protein binding in intercellular complexes, suggesting future avenues for investigation. Our findings offer insight into mechanisms of juxtacrine cell signalling and how tissue-scale properties emerge from individual cell behaviours.

15 # Introduction

16 Planar polarity and patterning of the insect cuticle

17 In multicellular organisms, cells in a tissue frequently adopt a common polarity such that they are
18 oriented in the same direction in the plane of the tissue. This is termed 'planar polarity' (or planar
19 cell polarity [PCP]) and is necessary for morphogenesis, for instance ensuring cells within a group
20 all move or intercalate along the same tissue axis. Furthermore, planar polarity is essential for
21 tissue function, for example when motile cilia on the surface of an epithelium all adopt the same
22 orientation and beat in the same direction (reviewed in Goodrich and Strutt, 2011; Devenport,
23 2014; Butler and Wallingford, 2017; Davey and Moens, 2017).

24 Cells within a tissue could each independently establish their planar polarity by reference to an
25 external cue such as a gradient of an extracellular signalling molecule, biasing protein localisations
26 to one or other side of a cell. Small biases could then be amplified through positive feedback to
27 generate strong polarity (Tree et al., 2002; Amonlirdviman et al., 2005; Le Garrec et al., 2006;
28 Abley et al., 2013; Warrington et al., 2017). However, variation in signal levels across the axis of a
29 cell might be small and difficult to discriminate, leading to individual cells mispolarising. A solution
30 is for cells to interact: comparing and coordinating polarity with their neighbours, thus establishing
31 uniform polarity across a field of cells even in cases where the external graded signal is weak or
32 noisy (Ma et al., 2003; Burak and Shraiman, 2009).

33 Evidence for cell-cell interactions during planar polarisation was provided by early transplantation
34 experiments (Piepho, 1955; Locke, 1959) and later by direct manipulation of underlying genetic
35 pathways in the fruit fly *Drosophila* (reviewed in Strutt, 2009). The best-studied pathway is known
36 as the 'core' pathway (Goodrich and Strutt, 2011; Aw and Devenport, 2017), which shows clear
37 evidence of cell-cell communication. However, some experimental results remain controversial,
38 leading to uncertainty about the nature of such 'signalling'.

39 The core planar polarity pathway

40 The core pathway has six known protein components, which physically interact to form intercellular
41 complexes at apicolateral cell junctions (Fig.1A). In planar polarised tissues, these complexes are
42 asymmetrically distributed to opposite cell ends. In the developing *Drosophila* wing, the sevenpass
43 transmembrane protein Fz localises to the distal side of cells (i.e. towards the tip of the wing) with
44 the cytoplasmic proteins Dishevelled (Dsh) and Diego (Dgo), whereas the fourpass
45 transmembrane protein Vang (also known as Strabismus [Stbm]) localises proximally (closest to
46 the hinge or body of the fly) with the cytoplasmic protein Prickle (Pk). The sevenpass
47 transmembrane atypical cadherin Flamingo (Fmi, also known as Starry Night [Stan]) forms
48 intercellular homodimers and localises both proximally and distally, bridging the two halves of the

complex (Strutt and Strutt, 2009) (Fig.1A). The asymmetric distribution of these proteins specifies the distal position from which an actin-rich hair, or trichome, emerges in each cell (Fig.1B).

Strikingly, non-cell autonomous activity within this pathway is observed when patches of cells lacking Fz activity are juxtaposed to cells with Fz activity during wing development. The *fz* mutant cells modify the polarity of their neighbours, whose trichomes point towards the *fz* mutant tissue (Gubb and Garcia-Bellido, 1982; Vinson and Adler, 1987). This is accompanied by relocalisation of the core proteins parallel to the clone boundary (Fig.1C) (Usui et al., 1999; Strutt, 2001; Bastock et al., 2003). Similarly, clones of cells lacking the activity of *Vang* alter the polarity of neighbouring cells, in this case causing their trichomes to point away from the mutant tissue (Fig.1D) (Taylor et al., 1998).

The reorganisation of polarity around clones of cells lacking Fz and Vang, and their colocalisation on apposing junctions, suggests direct roles for these proteins in cell-cell communication. However, loss of Fmi in clones results in loss of all other core components from junctions (including Fz and Vang) (Strutt, 2001; Feiguin et al., 2001; Axelrod, 2001; Tree et al., 2002; Bastock et al., 2003), but does not cause significant repolarisation of neighbouring cells (Usui et al., 1999; Chae et al., 1999). Furthermore, cells with altered Fz or Vang activity, but lacking Fmi, can no longer repolarise their neighbours, and cells lacking Fmi cannot be repolarised by neighbours with altered Fz or Vang activity (Lawrence et al., 2004; Strutt and Strutt, 2007; Chen et al., 2008). These data support the view that Fz-Fmi complexes in each cell interact with Fmi-Vang complexes in neighbouring cells, and these polarised molecular bridges are the conduits for cell-cell transmission of polarity information.

Core pathway signalling between cells: monodirectional or bidirectional?

While the involvement of Fz, Vang and Fmi in cell-cell signalling is well established, there has been considerable debate regarding whether information is transmitted between cells monodirectionally from Fz to Vang, or bidirectionally between Fz and Vang, with conflicting experimental data presented on each side.

Experiments in the *Drosophila* wing were designed to reveal the mechanism of signalling through examination of phenotypes around clones lacking both *Vang* and *fz* (Strutt and Strutt, 2007; Chen et al., 2008). It was hypothesised that should signalling be monodirectional from Fz-Fmi to Vang-Fmi, a double *Vang*$^-$ *fz*$^-$ clone would resemble a *fz*$^-$ single clone. In this scenario, neighbouring cells would not ‘sense’ the lack of Vang within the clone and would only be affected by the lack of Fz activity (Fig.1E). However, if signalling were bidirectional, neighbouring cells would no longer be able to send or receive information to/from clonal cells that lack both *Vang* and *fz* and would thus have normal polarity (Fig.1F). In experiments, *Vang*$^-$ *fz*$^-$ clones showed little or no non-autonomy, suggesting a bidirectional mechanism (Strutt and Strutt, 2007; Chen et al., 2008).

84 However, a later study suggested that *Vang*⁻ *fz*⁻ clones both qualitatively and quantitatively gave
85 the same phenotype as *fz*⁻ clones, supporting monodirectional signalling from Fz-Fmi to Fmi-Vang
86 (Wu and Mlodzik, 2008). Taken together with biochemical data revealing a physical interaction
87 between Fz and Vang, the authors concluded that Fz is a ligand for Vang, which acts as a receptor
88 for polarising signals.

89 In studies on *Drosophila* abdomen hair polarity, it was also suggested that Fz-Fmi in one cell
90 signals monodirectionally to Fmi-Vang in the next (Lawrence et al., 2004). However, on revisiting
91 this work, Lawrence and colleagues concluded that an experimental artefact had misled them
92 (Struhl et al., 2012) and a further series of experiments instead supported bidirectional signalling.

93 While the weight of evidence suggests bidirectional signalling is the likely mechanism, the
94 conclusions drawn, particularly regarding experiments in the *Drosophila* wing, remain
95 controversial. Furthermore, *fmi*⁻ single clones have been shown experimentally to show no non-
96 autonomy in most cases and weak proximal non-autonomy in some examples (Chen et al., 2008;
97 Le Garrec et al., 2006; Strutt and Strutt, 2007), but the mechanisms discussed here do not make
98 predictions about the *fmi*⁻ clone phenotype within the context of mono- or bi- directional signalling.

99 Mechanisms of feedback amplification of polarity

100 To generate a strongly polarised system, it is thought that small biases in protein localisation are
101 induced by global cues (e.g. gradients), which are then amplified by positive feedback (Aw and
102 Devenport, 2017). Such feedback is most commonly assumed to occur through 'like' complexes of
103 the same orientation stabilising each other, and/or 'unlike' complexes of opposite orientations
104 destabilising each other (Fig.1G). Both interactions are hypothesised to result in a local build-up of
105 complexes of the same orientation (Klein and Mlodzik, 2005; Strutt and Strutt, 2009).

106 The non-transmembrane core pathway components, Dsh, Pk and Dgo, are required for
107 amplification of polarity by promoting segregation of the core protein complexes to proximal and
108 distal cell edges. Thus loss of their activity in clones of cells results in a failure of the mutant cells
109 to planar polarise. However, this does not cause significant repolarisation of neighbouring wild-type
110 cells (Gubb et al., 1999; Theisen et al., 1994; Amonlirdviman et al., 2005; Strutt and Strutt, 2007).

111 A number of molecular mechanisms have been proposed to mediate such stabilising and
112 destabilising interactions. As core proteins progressively localise into clusters of the same
113 orientation during polarisation, it has been suggested that 'like' complexes may intrinsically cluster
114 (Strutt et al., 2011; Cho et al., 2015) and that this may be driven by multiple low-affinity interactions
115 between core proteins leading to a phase transition into a stable state (Strutt et al., 2016).
116 Conversely, destabilising interactions have been proposed to occur via Pk-Vang inhibiting Dsh
117 binding to Fz (Tree et al., 2002; Amonlirdviman et al., 2005; Jenny et al., 2005), or by Pk reducing

118 Dsh-Fz stability (Warrington et al., 2017), or by Fz-Dsh promoting Pk-mediated internalisation and
119 turnover of Vang (Cho et al., 2015). Since such mechanisms suggest an effect on the stability of
120 *inter*cellular complexes this might predict a role in altering signalling between cells, although the
121 relationship between feedback and signalling directionality has not previously been examined.

122 Computational modelling of planar polarity

123 Numerous computational models have been proposed, implementing a variety of different
124 feedback interactions between core protein complexes, all of which successfully recapitulate a
125 polarised state (e.g. Amonlirdviman et al., 2005; Le Garrec et al., 2006; Burak and Shraiman,
126 2009; Schamberg et al., 2010). However, while these models have generally attempted to
127 reproduce single clone phenotypes, none have examined double clones or mechanisms of cell-cell
128 signalling directionality. Furthermore, while it appears evident that core protein asymmetric
129 distributions driven by feedback amplification are intrinsically linked to cell-cell signalling and
130 propagation of planar polarity, the relationship between these phenomena remains largely
131 unexplored.

132 To address these issues, we have used computational modelling to explore different scenarios for
133 core pathway function, based on different assumptions regarding protein behaviours. This, taken
134 together with new experimental data to reassess the *Vang*$^{-}$ *fz*$^{-}$ clone phenotype, allows us to make
135 strong predictions regarding likely molecular mechanisms of action and provides the basis for
136 future experimental studies.

137 Results and Discussion

138 A computational modelling framework for investigating cell-cell signalling and feedback
139 amplification in planar polarity

140 We developed a computational framework to model potential molecular mechanisms for planar
141 polarity signalling. The framework represents a simplified system, to allow rapid testing of different
142 signalling regimes and simulation of clone phenotypes.

143 Within this framework, Fz and Vang each represent both the transmembrane protein encoded by
144 the corresponding gene, and the associated cytoplasmic proteins with which they interact and
145 which are required for feedback amplification of protein asymmetry. Thus, 'Fz' represents Fz
146 bound to Dsh and Dgo, and 'Vang' represents Vang associated with Pk. Fmi is allowed to bind
147 homophilically in trans between neighbouring cells (indicated by ':' in later text), and also to interact
148 in cis with either Fz or Vang in the membranes of the same cell (indicated by '-' in later text;
149 Fig.S1A).

150 Planar polarity was simulated in a one-dimensional row of cells, each with two compartments
151 representing proximal (left) and distal (right) sides of the cell membrane, respectively (Fig.S1B).
152 The system was initialised with one arbitrary unit (AU) of each molecular species per compartment
153 at the start of each simulation, except with a small imbalance in initial Fz level towards distal sides
154 of cells to provide a global orienting cue, which could be amplified by feedback interactions. Wild-
155 type polarity was defined as higher Fz bound into complexes at distal cell ends and higher Vang
156 bound at proximal cell ends (Fig.S1C).

157 As discussed, there is evidence for two forms of intracellular feedback interactions: local
158 destabilisation of 'unlike' oriented complexes, and local stabilisation of 'like' oriented complexes
159 (Fig.1G). Destabilising feedback interactions were implemented such that Vang-containing
160 complexes (Vang-Fmi:Fmi, Vang-Fmi:Fmi-Fz and Vang-Fmi:Fmi-Vang) in each cell compartment
161 destabilised Fz-containing complexes (Fz-Fmi:Fmi, Fz-Fmi:Fmi-Vang, Fz-Fmi:Fmi-Fz) in the same
162 compartment, and vice versa. The strengths of destabilising feedbacks from Fz and Vang were
163 given by the parameters $V_{max,F}$ and $V_{max,V}$, respectively, representing the maximum fold-change
164 conferred to the off-rate of each reaction (see Experimental Procedures and Supplemental Text).
165 Stabilising feedback interactions were implemented in a similar manner, by modulating reaction
166 on-rates, with Vang- or Fz-containing complexes stabilising themselves.

167 After exploring both destabilising and stabilising feedback interactions in simulations, we
168 concluded that in general these mechanisms polarised the system equivalently. However, while
169 stabilising feedbacks recapitulated key clone phenotypes, there were subtle differences in some
170 cases (e.g. Fig.S1D; Supplemental Text for further discussion). In particular, for systems relying
171 only on stabilising feedbacks, 'unlike' complex stability was unchanged, thus the system was
172 slower to polarise and more sensitive to the rate of protein diffusion to sort complexes. Hereafter,
173 we describe models with destabilising feedbacks only. Since molecular evidence for local
174 destabilising feedback interactions both from Fz to Vang and from Vang to Fz have been reported
175 in the literature (Tree et al., 2002; Jenny et al., 2005; Cho et al., 2015; Warrington et al., 2017),
176 both were implemented in these models, unless otherwise stated, by setting the values of $V_{max,F}$
177 and $V_{max,V}$ to greater than 1 (see Experimental Procedures; Fig.1H).

178 A set of ordinary differential equations describing the binding and diffusion events that occur in
179 complex formation and localisation (Fig.S1B), were numerically solved and allowed to evolve to
180 steady state (Supplemental Text).

181 We designed models with different signalling assumptions, namely 'no direct signalling' (Model 1),
182 'direct monodirectional signalling' (Model 2) or 'direct bidirectional signalling' (Model 3). While the
183 molecular nature of such cell-cell signalling remains unclear, we have assumed that polarity
184 information is transmitted directly via mass-action binding of complexes at intercellular junctions.
185 To implement this we introduced variations in the relative dissociation constants of complexes,

186 indicating how a cell may be able to directly 'sense' the presence of Fz or Vang in its neighbours
187 when complexes form. For example in the no direct signalling model, both Fz and Vang were
188 allowed to bind to and stabilise Fmi:Fmi dimers, such that all complexes involving Fz or Vang had
189 equal K_D (Fig.2A). Thus, Fz and Vang could not promote each other's incorporation into
190 intercellular complexes and therefore could not 'send' information to neighbouring cells.

191 We tested each model's ability to reproduce the following experimental observations:

192 (i) polarisation of Fz and Vang in wild-type tissue;
193 (ii) reversal of polarity in the 5-10 cells neighbouring those in a clone lacking the activity of
194 *fz* or *Vang*;
195 (iii) no reversal of polarity in cells neighbouring a *fmi*$^-$ clone.

196 Models that met each of these criteria were then used to predict the phenotype of *Vang*$^-$ *fz*$^-$ double
197 clones, and these predictions were then tested experimentally. We quantified non-autonomy
198 around a clone as the number of cells with reversed polarisation in terms of Fz localisation (in
199 general results were the same if we instead considered Vang localisation [e.g. Fig.3B]). Reversals
200 of polarity in cells to the right of a clone, such that Fz pointed towards the clone, was termed distal
201 non-autonomy (i.e. a *fz*-like phenotype), while polarity reversals to the left were termed proximal
202 non-autonomy (*Vang*-like).

203 A model with no direct signalling is unable to reproduce non-autonomy around *fz*$^-$ and *Vang*$^-$
204 clones (Model 1)

205 We first assessed whether direct signalling is required to establish polarity in our modelling
206 framework by simulating complex formation with no direct communication between cells. We
207 termed this model 'no direct signalling' (Table 1: Model 1; Fig.2), indicating that a cell is unable to
208 directly 'sense' the presence of Fz or Vang in its neighbours when complexes form. As discussed
209 previously, this is achieved by implementing equal K_D for complex formation in reactions 2-7
210 (Fig.2A). Thus, Fz and Vang do not directly promote each other's incorporation into intercellular
211 complexes.

212 We established parameter values (see Supplemental Text) for which Model 1 generated wild-type
213 polarity (Fig.2B), thus meeting criterion (i). We then examined the behaviour of loss-of-function
214 clones in this model. We hypothesised that under the 'no signalling' assumption, this model would
215 not generate non-autonomy around clones of cells with altered Fz or Vang activity.

216 Indeed, we found no non-autonomy around *fz*$^-$ or *Vang*$^-$ clones (Fig.2C,D), thus this model failed
217 to meet criterion (ii). Increasing the strength of feedback did not result in non-autonomy around
218 such clones, while decreasing it below a threshold resulted in no polarisation. To rationalise this,
219 we consider the possible complexes that can form on the boundary of a *fz*$^-$ clone. Allowing all

220 complexes to form with equal affinity leads to equal amounts of Fz and Vang on the outer clone
221 boundary and thus no preferential accumulation of either protein over the other (Fig.S2A). In this
222 model, since Fz or Vang binding in one cell is not influenced by availability of Fz or Vang in a
223 neighbouring cell, in cells outside the clone the initial bias in unbound Fz levels is the driving force
224 for feedback-amplified polarisation.

225 We next relaxed our simplifying assumption that feedback interactions act with equal strength and
226 examined the model with unbalanced feedbacks ($V_{max,F} \neq V_{max,V}$) or with just a single feedback
227 (where either $V_{max,F}$ or $V_{max,V}$ are 1). For the initial Fz bias considered, simulations revealed that the
228 model failed to polarise if feedbacks were unbalanced (e.g. Fig.S2B,C). Based on its inability to
229 reproduce observed *fz*⁻ and *Vang*⁻ clone phenotypes, we rejected Model 1, and proceeded to
230 consider the effect of direct signalling.

231 A direct monodirectional signalling model reproduces non-autonomous phenotypes around *fz*⁻,
232 *Vang*⁻ and *fmi*⁻ clones and predicts distal non-autonomy around *Vang*⁻ *fz*⁻ double clones (Model 2)

233 We next implemented 'direct monodirectional signalling' (Table 1: Model 2; Fig.3), from Fz to Vang,
234 such that Vang bound more strongly to a Fmi:Fmi-Fz complex (i.e. a low dissociation constant;
235 Fig.3A, reaction 4) than to just Fmi:Fmi (Fig.3A, reaction 3), thereby 'sensing' the presence of Fz in
236 the neighbouring cell. In contrast, Fz bound to a Fmi:Fmi-Vang complex (Fig.3A, reaction 5) had
237 the same intermediate dissociation constant as Fz bound to just Fmi:Fmi (Fig.3A, reaction 2). Thus
238 localisation of Vang at junctions was promoted by Fz in the next cell, but Fz was unaffected by
239 Vang in the next cell (Fig.3A). As for Model 1, we considered polarity to be amplified by mutually
240 destabilising feedback interactions, initially acting with equal strength (see Fig.1H).

241 Monodirectional signalling resulted in polarisation of wild-type cells and furthermore, reproduced
242 the experimentally observed distal and proximal non-autonomy around *fz*⁻ and *Vang*⁻ clones,
243 respectively, for a range of feedback strengths (Fig.3B-E), thus meeting criteria (i) and (ii). We
244 rationalise this by considering that Vang binds preferentially to complexes containing Fz in the next
245 cell. Thus, in cells immediately neighbouring a *fz*⁻ clone, Vang preferentially localises away from
246 the clone (Fig.S3A) which results in reversed polarity distal to the clone.

247 The range of non-autonomy was a function of the strength of feedbacks (V_{max}, where $V_{max} = V_{max,F}$
248 $= V_{max,V}$). Higher values of either parameter suppressed non-autonomy, since the amplification of
249 the initial bias in each cell dominated over the mislocalisation of protein complexes propagating
250 from the clone edge (Fig.3C,E; see Supplemental Text).

251 Simulations revealed that our model of direct monodirectional signalling showed distal non-
252 autonomy around *fmi*⁻ clones for a range of feedback strengths (Fig.3F,G) and therefore did not
253 recapitulate experimental observations in the fly wing. We note that in the first cell neighbouring

254 the clone, neither Vang nor Fz could bind at the clone boundary (Fig.3F). Thus, since we have
255 quantified non-autonomy via Fz localisation, the first cell proximal to the clone is also scored as
256 non-autonomous (Fig.3G).

257 To rationalise the distal non-autonomy, we consider complexes that can form at a *fmi*$^-$ clone
258 boundary (Fig.S3B). In cells immediately next to the clone, both Fz and Vang localise away from
259 the clone. However, Vang preferentially binds to Fz-containing complexes and thus accumulates
260 on the boundary furthest from the clone to higher levels than Fz and this difference is amplified by
261 the feedback interactions (Fig.S3B, orange arrows), leading to distal non-autonomy. The failure to
262 mimic experimental observations led us to reject Model 2 under the conditions of balanced
263 feedbacks.

264 We next relaxed our simplifying assumption that feedback interactions act with equal strength and
265 examined the model with unbalanced feedbacks ($V_{max,F} \neq V_{max,V}$) or with just a single feedback
266 (where either $V_{max,F}$ or $V_{max,V}$ are 1). Simulations revealed that this model could no longer generate
267 a polarised steady state when feedback was stronger from Vang ($V_{max,F} < V_{max,V}$), or with either
268 feedback operating alone, thereby failing to meet criterion (i). However, with stronger feedback
269 acting from Fz complexes to destabilise Vang binding ($V_{max,F} > V_{max,V}$, where $V_{max,V} \geq 5$; e.g.
270 Fig.3H), this model generated a polarised steady state and recapitulated the phenotypes of *fz*$^-$ and
271 *Vang*$^-$ (Fig.3I,J). For a limited parameter range ($V_{max,F} = 15$, $V_{max,V} = 5$), this model also generated
272 autonomous *fmi*$^-$ clones (Fig.3K), thereby meeting all of our criteria.

273 Having found conditions (i.e. with stronger feedback from Fz) under which the direct
274 monodirectional signalling model could reproduce criteria (i)-(iii), we then used it to predict the
275 phenotype of *Vang*$^-$ *fz*$^-$ double clones, for which experimental results remain controversial (Strutt
276 and Strutt, 2007; Chen et al., 2008; Wu and Mlodzik, 2008). Simulations revealed distal non-
277 autonomy around such double clones (Fig.3L). In cells immediately neighbouring *Vang*$^-$ *fz*$^-$ clones,
278 Vang preferentially binds to Fz-containing complexes and thus accumulates on the boundary
279 furthest from the clone (Fig.S3C, orange arrows). Based on these simulated clone phenotypes, we
280 conclude that Model 2 may be a valid model of planar polarisation in the fly wing if feedback is
281 stronger from the Fz side of the complex, and it predicts distal non-autonomy around *Vang*$^-$ *fz*$^-$
282 double clones.

283 A direct bidirectional signalling model reproduces non-autonomous phenotypes around *fz*$^-$, *Vang*$^-$
284 and *fmi*$^-$ clones and predicts no non-autonomous polarity around *Vang*$^-$ *fz*$^-$ double clones (Model
285 3)

286 An alternative mechanism of signalling that has been presented in the literature is that of
287 bidirectional signalling. We next established a model of 'direct bidirectional signalling' (Table 1:
288 Model 3; Fig.4) to address whether it too could meet our criteria of generating a polarised steady

289 state and reproducing single clone phenotypes. In this model both Vang bound to a Fmi:Fmi-Fz
290 complex (Fig.4A, reaction 4) and Fz bound to a Fmi:Fmi-Vang complex (Fig.4A, reaction 5) had
291 low dissociation constants, but Vang bound to Fmi:Fmi (Fig.4A, reaction 3) and Fz bound to
292 Fmi:Fmi (Fig.4A, reaction 2) had intermediate dissociation constants. Thus Fz and Vang both
293 promoted each other's binding in the next cell (Fig.4A). As for our previous models, we considered
294 amplification to be mediated by mutually destabilising feedback interactions, initially acting with
295 equal strengths (see Fig.1H).

296 In this model the expected distal and proximal non-autonomy were observed around *fz*$^-$ and *Vang*$^-$
297 clones, respectively (Fig.4B-E). We rationalise these phenotypes by considering the complexes
298 that can form in the cells immediately neighbouring the clone. For example, in cells next to a *fz*$^-$
299 clone, Vang preferentially localises towards cells expressing its binding partner, Fz. Since there is
300 no Fz within the clone, Vang accumulates on boundaries furthest from the clone (Fig.S4A, orange
301 arrows). This model also recapitulated the expected phenotype of *fmi*$^-$ clones, for which neither Fz
302 nor Vang binding is favoured at clone boundaries, resulting in no propagating non-autonomy
303 (Fig.4F,G; Fig.S4B).

304 Since the direct bidirectional signalling model accurately reproduced *fz*$^-$, *Vang*$^-$ and *fmi*$^-$ clone
305 phenotypes, meeting criteria (i)-(iii), we used this model to predict the phenotype of *Vang*$^-$ *fz*$^-$
306 double clones. In contrast to the direct monodirectional model, it predicted no non-autonomous
307 polarity around *Vang*$^-$ *fz*$^-$ double clones (Fig.4H,I). Considering the complexes that can form at this
308 clone boundary, both Fz and Vang can form trimer complexes on the edge of the clone, but these
309 are less favoured than tetramer complexes. Thus both Fz and Vang preferentially localise to the
310 boundary furthest from the clone where neither is favoured over the other (Fig.S4C). Polarity
311 direction is thus driven by the initial bias in Fz localisation, not by the clone.

312 To examine whether our findings depended on our simplifying assumption that feedback
313 interactions act with equal strength, we relaxed this assumption and examined the model with
314 unbalanced feedbacks ($V_{max,F} \neq V_{max,V}$; for example Fig.4J) or with just a single feedback (where
315 either $V_{max,F}$ or $V_{max,V}$ are 1). If only a single feedback was present, the system did not polarise. In
316 the case of unbalanced feedbacks, single *fz*$^-$ or *Vang*$^-$ clones behaved as expected, with distal and
317 proximal non-autonomy (Fig.4K,L), respectively.

318 For strong differences in feedback strength (i.e. $V_{max,F} = 5$, $V_{max,V} > 8$ or $V_{max,V} = 5$, $V_{max,F} > 8$), *fmi*$^-$
319 clones exhibited non-autonomy (Fig.4M), thus failing to meet criterion (iii). In cells neighbouring
320 *fmi*$^-$ clones, the immediate boundary is unable to localise any complexes due to the inability to
321 form Fmi:Fmi dimers. Since all of the proteins in such cells must localise to the boundary furthest
322 from the clone, the protein mediating the feedback 'wins' on this boundary (Fig.S5A). For instance,
323 Fz accumulates on the boundary furthest from the clone when it more strongly destabilises Vang,
324 and Vang accumulates away from the clone when it strongly destabilises Fz. In contrast, for weak

325 differences in feedback strength (e.g. $V_{max,F}$ = 5, $V_{max,V}$ = 8) little non-autonomy was observed in
326 cells neighbouring *fmi*⁻ clones (Fig.4M), thus meeting criterion (iii). We therefore examined the
327 phenotype predicted for *Vang*⁻ *fz*⁻ double clones under these conditions. They showed distal non-
328 autonomy when feedback was slightly stronger from Fz, but proximal non-autonomy when
329 feedback was slightly stronger from Vang (Fig.4N; Fig.S5B).

330 Based on these simulated clone phenotypes, we conclude that Model 3 may be a valid model of
331 planar polarisation in the fly wing. If feedback is balanced between the two sides of the complex,
332 criteria (i)-(iii) are met and no non-autonomy is predicted around *Vang*⁻ *fz*⁻ double clones.
333 However, all criteria are also met if feedbacks are weakly unbalanced, but this leads to distal or
334 proximal non-autonomy around *Vang*⁻ *fz*⁻ double clones depending on which feedback is
335 strongest.

336 The absence of symmetric complex formation leads to indirect signalling (Model 4)

337 Notably there is no experimental evidence to rule out the formation of symmetric complexes (Fz-
338 Fmi:Fmi-Fz and Vang-Fmi:Fmi-Vang), and visualising the structure of individual complexes is
339 beyond the limits of conventional microscopy. Therefore, we allowed symmetric complexes to form
340 in Models 1-3. However, previously published computational models have assumed that symmetric
341 complexes do not form (Amonlirdviman et al., 2005; Le Garrec et al., 2006; Burak and Shraiman,
342 2009). To test whether this difference was important, we adapted our model with no direct
343 signalling (Model 1), to block the formation of symmetric complexes (Table 1: Model 4; Fig.5). This
344 was achieved by setting the relevant binding rate constants (k_6, k_7) to zero (Fig.5A). We first
345 confirmed that this model could generate stably polarised cells through amplification of the initial
346 global cue by local destabilising feedback interactions both from Fz to Vang and from Vang to Fz
347 (Fig.5B), thereby meeting criterion (i).

348 We next introduced clones into the model. In agreement with previous modelling work and despite
349 the lack of direct signalling across complexes, we found that *fz*⁻ clones showed distal non-
350 autonomy (Fig.5C) and *Vang*⁻ clones showed proximal non-autonomy (Fig.5D), thereby meeting
351 criterion (ii). To illustrate the consequences of only allowing asymmetric complexes to form, we
352 consider the example of a *fz*⁻ clone. On the boundary between a *fz*⁻ clone and a neighbouring wild-
353 type cell, only Vang can bind to Fmi:Fmi on the inner clone boundary. At the outer clone boundary
354 Fz binding is favoured over Vang binding (as Vang-Fmi-Fmi-Vang complexes could not form,
355 Fig.5E). This generates an imbalance whereby more Fz can bind to the outer clone boundary than
356 Vang and this difference can be amplified by feedback interactions (Fig.5E).

357 Simulations revealed that *fmi*⁻ clones were autonomous for this model (Fig.5F). Since this model
358 was able to reproduce all single clone phenotypes meeting criteria (i)-(iii), we went on to use it to

359 predict the outcome of *Vang*⁻ *fz*⁻ clones. Such clones were autonomous (Fig.5G), mimicking the
360 findings of the direct bidirectional signalling mode (Model 3).

361 We next relaxed our assumption that feedbacks operate with equal strengths and examined the
362 model with unbalanced feedbacks ($V_{max,F} \neq V_{max,V}$; for example Fig.5H) or with just a single
363 feedback (where either $V_{max,F}$ or $V_{max,V}$ are 1). If only a single feedback was present, the system did
364 not polarise. We found that single *fz*⁻ or *Vang*⁻ clones behaved as expected when feedbacks were
365 unbalanced (Fig.5I,J).

366 As for Model 3, weak differences in feedback strength (e.g. $V_{max,F} = 4$, $V_{max,V} = 6$ or $V_{max,F} = 6$,
367 $V_{max,V} = 4$) resulted in little non-autonomy in cells neighbouring *fmi*⁻ clones (Fig.5K), and criteria (i)-
368 (iii) were all met. Thus, we examined the phenotype predicted for *Vang*⁻ *fz*⁻ double clones under
369 these conditions, finding them to show proximal non-autonomy when feedback from Vang was
370 stronger, but distal non-autonomy when feedback from Fz was stronger (Fig.5L). For stronger
371 differences in feedback strength, *fmi*⁻ clones exhibited non-autonomy (Fig.5K), thus failing to meet
372 criterion (iii).

373 We conclude that Model 4 may be a valid model of planar polarity in the fly wing and that the
374 presence of two opposing feedback interactions results in 'indirect bidirectional signalling' (with the
375 balance of the feedbacks determining the balance of the directionality).

376 To summarise our findings so far, we can find regions in parameter space for the direct
377 monodirectional (Model 2), direct bidirectional (Model 3) and indirect bidirectional (Model 4) models
378 that recapitulate *fz*⁻, *Vang*⁻ and *fmi*⁻ single clone phenotypes. However, these models predict
379 qualitative differences in the phenotype around *Vang*⁻ *fz*⁻ double clones. To constrain our models
380 and identify the most likely mechanism of planar polarity signalling in the wing, we re-examined the
381 *Vang*⁻ *fz*⁻ double clone phenotype.

382 <u>The non-autonomous phenotype of *fz*⁻ clones is suppressed by simultaneous loss of *Vang*</u>

383 As the *fz* and *Vang* genes lie on different chromosomes, previous studies generated clones of
384 double-mutant tissue using transgenes that artificially provided *fz* or *Vang* function on a different
385 chromosome arm. These studies used exogenous promoters, which might not provide identical
386 activity levels to the endogenous genes (Strutt and Strutt, 2007; Chen et al., 2008; Wu and
387 Mlodzik, 2008). Thus in each study, cells lacking Fz and Vang activity are juxtaposed to
388 neighbours with potentially differing levels of Fz and Vang activity, and this may explain the varying
389 degrees of non-autonomous propagation of polarity reported in each case.

390 To circumvent the disadvantages inherent in this approach, we generated *fz*⁻ clones in which Vang
391 activity was either normal or was reduced only within the cells of the clone using RNAi in a
392 MARCM GAL4/GAL80-dependent strategy (Lee and Luo, 1999 see Experimental Procedures). In

393 this method, GAL80 suppresses expression of the RNAi transgene in all tissue except for the clone
394 tissue. No transgenes were used to substitute for Fz or Vang activity, and thus the different clone
395 genotypes should be directly comparable.

396 Control *fz*⁻ clones in the pupal wing, examined shortly before or around the time of trichome
397 formation, showed the expected strong Fz and Vang localisation at clone boundaries (Fig.6A,
398 white arrowheads). Propagation of this aberrant polarity extended around 5-10 cells into
399 neighbouring tissue with associated mispolarisation of trichomes pointing towards clone tissue
400 (Fig.6B, arrows, Vinson and Adler, 1987; Strutt, 2001; Bastock et al., 2003).

401 In *fz*⁻ clones, expressing a *UAS-Vang-RNAi* transgene caused loss of immunoactivity for Vang
402 protein (Fig.6C). There was no notable effect on trichome polarity outside the clones (Fig.6D) and
403 consistent with this, Fz and Vang recruitment to the clone boundary (Fig.6C, white arrowheads)
404 from other cell edges (Fig.6C, yellow arrowheads) was suppressed (Fig.6E).

405 We further considered whether the differences seen in previous reports were due to the stage at
406 which trichome polarity was assayed, as two reports looked at pupal stages (Strutt and Strutt,
407 2007; Chen et al., 2008) and one analysed adult wings (Wu and Mlodzik, 2008). However, looking
408 in adult wings in which Vang activity in *fz*⁻ clones was reduced by RNAi, we again observed a
409 strong suppression of non-autonomy (compare Fig.6F,G to Fig.6H,I).

410 Thus, reduction in Vang activity in *fz*⁻ clones reduces Fz and Vang localisation at clone
411 boundaries, and reduces propagation of polarity defects outside the clone, supporting previous
412 reports that the non-autonomy of *Vang*⁻ *fz*⁻ clones is suppressed as compared to *fz*⁻ clones (Strutt
413 and Strutt, 2007; Chen et al., 2008). Together with our modelling predictions this suggests that
414 signalling is bidirectional. Thus we reject Model 2 and conclude that Models 3 and 4 are plausible
415 models of planar polarity signalling in the wing.

416 **Conclusions**

417 We set out to understand the possible molecular wirings that might underlie the cell-cell
418 coordination of planar polarity. We specifically address possible scenarios that would explain the
419 observed behaviour of the core planar polarity pathway in the *Drosophila* wing, but our findings
420 also reveal other scenarios that could coordinate polarity in other contexts.

421 We developed a suite of models reflecting different 'signalling' regimes that could reproduce a wild-
422 type polarised steady state and single clone phenotypes (Table 1). Our monodirectional and
423 bidirectional signalling models were able to produce polarised tissue and reproduce the
424 phenotypes of single mutant *fz*⁻ and *Vang*⁻ clones. Interestingly, monodirectional and bidirectional
425 models made different predictions about the feedback interactions necessary to reproduce the
426 autonomy of *fmi*⁻ clones. Namely, monodirectional signalling from Fz to Vang required that

427 feedback be stronger from Fz than Vang, while bidirectional signalling required that feedbacks be
428 balanced (or only weakly unbalanced).

429 Under such conditions, monodirectional and bidirectional models made different predictions about
430 the *Vang*$^{-}$ *fz*$^{-}$ double clone phenotype, either predicting distal non-autonomy or complete
431 autonomy. By carrying out new experiments examining the double *Vang*$^{-}$ *fz*$^{-}$ clone phenotype in
432 the wing, we confirm that non-autonomy is suppressed when compared to either *fz*$^{-}$ or *Vang*$^{-}$
433 single mutant clones. This supports the conclusion that signalling between Fz and Vang is
434 bidirectional and that feedback interactions are balanced, with Models 3 and 4 thus being the most
435 plausible.

436 Interestingly, simulations revealed that bidirectional signalling could be mediated either *indirectly*
437 via intrinsically asymmetric intercellular protein complexes and bidirectional feedbacks, or *directly*
438 via different affinities for protein binding in intercellular complexes. Both models behaved similarly
439 in that they required balanced feedback between Fz and Vang to reproduce the expected *fmi*$^{-}$ and
440 double *Vang*$^{-}$ *fz*$^{-}$ clone phenotypes.

441 Overall, our work suggests that while many binding and feedback regimes can generate polarity
442 and reproduce *fz*$^{-}$ and *Vang*$^{-}$ single clone phenotypes, *Vang*$^{-}$ *fz*$^{-}$ double clones and *fmi*$^{-}$ clones are
443 key simulations required to constrain model parameters to mirror the *in vivo* reality and apparent
444 symmetry in the system.

445 We suggest that future experimental studies should focus on two questions. First, what are the
446 molecular parameters of intercellular complex formation and do these support formation of
447 intrinsically asymmetric complexes and/or direct signalling between Fz and Vang? Second, what is
448 the molecular nature of the feedback interactions and can at least two opposing feedbacks be
449 identified between Fz- and Vang-containing complexes?

450 **Experimental Procedures**

451 *Drosophila genetics*

452 Mitotic clones were generated using the *fz*^{P21} allele, which is considered to be a null (Jones et al.,
453 1996), using the MARCM system (Lee and Luo, 1999) and *Ubx-FLP* (Emery et al., 2005). Here,
454 *tub-GAL4* and *UAS-GFP* were expressed in every cell, but *tub-GAL80* suppressed expression of
455 *UAS-GFP* in heterozygous or twin-spot tissue only, thus GFP was only observed in *fz*$^{-}$ clone cells.
456 To generate *Vang*$^{-}$ *fz*$^{-}$ double clones, *UAS-Vang-RNAi* transgenes were introduced distal to *fz* on
457 chromosome 3L, such that they also would only be expressed within clones. Strength of Vang
458 knockdown was visualised by staining for Vang. Figures show results from a line from the TRiP
459 collection (HMS01343). However, to control for potential off-target effects, results were confirmed
460 with a non-overlapping independent *pWIZ* line (Bastock and Strutt, 2007). Full genotypes were:

461 Fig. 6A,B,F,G:

462 *Ubx-FLP tubGAL4 UAS-nGFP/+ ; fz^{P21} FRT80 / tubGAL80 FRT80*

463 Fig. 6C,D,H,I:

464 *Ubx-FLP tubGAL4 UAS-nGFP/+ ; UAS-Vang-RNAi$^{(TRiP)}$ fz^{P21} FRT80 / tubGAL80 FRT80*

465 *Dissection and Immunohistochemistry*

466 White prepupae were collected and aged as appropriate at 25°C. Pupal wings were dissected at
467 either 28 h APF to visualise polarity protein localisation, or at 32.25 h APF for trichomes. Pupal
468 wings were then fixed and stained as previously described (Warrington et al., 2017). Briefly, pupae
469 were fixed for 30-45 minutes at room temperature, prior to dissection of the pupal wing. Wings
470 were transferred into PBS containing 0.2% Triton X-100 (PTX) and 10% normal goat serum to
471 block prior to antibody incubation. Wings were incubated with antibodies overnight at 4°C, and
472 mounted in 10% glycerol, 1xPBS, containing 2.5% DABCO (pH7.5). Primary antibodies for
473 immunostaining were affinity purified rabbit anti-GFP (ab6556, Abcam, UK), affinity-purified rabbit
474 anti-Fz (Bastock and Strutt, 2007), rat anti-Vang (Strutt and Strutt, 2008) and mouse monoclonal
475 anti-Fmi (Flamingo #74, DSHB, (Usui et al., 1999)). Trichomes were stained using Phalloidin
476 conjugated to Alexa-568 (Molecular Probes). Adult wings were dissected from newly eclosed flies
477 and transferred to a 10 µl drop of PTX in a depression slide for imaging.

478 *Imaging*

479 Fixed pupal wings were imaged on a Nikon A1R GaAsP confocal microscope using a 60x NA1.4
480 apochromatic lens, with a pixel size of 138 nm, and the pinhole was set to 1.2 AU. 9 Z-slices
481 separated by 150 nm were imaged, and then the 3 brightest slices around junctions were selected
482 and averaged for each channel in ImageJ. Adult wings were imaged on a fluorescence compound
483 microscope to capture trichomes in brightfield and GFP to mark clonal cells. Since brightfield and
484 GFP signals were in different planes, single slices were selected and realigned in Adobe
485 Photoshop.

486 *Computational modelling*

487 A detailed description of the model equations, assumptions, conditions, and parameters can be
488 found in the Supplemental Text. Briefly, the computational model comprises a set of coupled
489 ordinary differential equations, which encode intercellular binding reactions between core
490 proteins/complexes and intracellular diffusion in a one-dimensional looped line of cells aligned
491 along a proximodistal axis. This set of equations is solved numerically using an explicit Runge-
492 Kutta method. A MATLAB implementation will be deposited in GitHub. Steady state was
493 considered to be achieved once levels of all molecular species remained constant after solving for

494 a sufficiently long time (for example see Fig.S1E,F). Wild-type polarity was defined as higher levels
495 of bound Fz on distal cell edges with higher levels of Vang on proximal cell edges and generally
496 these differences were strong when such bistability occurred.

497 A brief description of key model parameters is given here:

498 *Binding rate constants:* Mass action binding rates are proportional to the product of reactants in
499 any reaction. Forward reaction rates are parameterised by rate constants k_1 to k_7, and reverse
500 reactions by v_1 to v_7. The relative reaction rates are thus determined by the dissociation constant
501 K_D calculated by v_j/k_j.

502 *Diffusion:* In a 1D model where each cell has just two compartments, diffusion is modelled by a
503 linear flux between these compartments. The rate of this flux is parameterised by $D = \mu/L^2$, where μ
504 is the diffusion coefficient, estimated at 0.03 $\mu m^2 s^{-1}$ (Fischer et al., 2013; Klünder et al., 2013) and
505 L is the distance between compartments, estimated at 5 µm.

506 *Feedback:* Destabilising feedback is modelled by a Hill function of the form $h(x) = 1 + (V_{max} -$
507 $1)[x]^w/(K^w + [x]^w)$, where $[x]$ is the amount of protein x mediating the feedback.

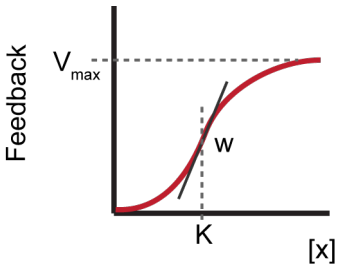

The parameter V_{max} determines the strength of the feedback as the maximum fold-change that can be conferred to the off-rate of each reaction. Since feedback can be mediated by either Fz or Vang, strength of feedback is determined by $V_{max,F}$ or $V_{max,V}$, respectively. K determines the amount of protein x required to switch from weak to strong feedback and w determines the rate of this switch. We set K to 0.5, which is half of the initial concentration of Fz and Vang in each compartment. A higher value of w reflects cooperativity such that a small increase in $[x]$ can cause large differences in its ability to destabilise complexes. Since we do not have evidence of enzymatic ability in these reactions which may cause such cooperativity, we aimed to maintain w as low, and is thus set to 2 in all simulations shown.

Acknowledgements

The authors would like to thank Guy Blanchard, Jochen Kursawe, Helen Strutt and Simon Fellgett for comments on the manuscript. We also acknowledge the Bloomington *Drosophila* Stock Center for providing fly strains. The work was funded by a Wellcome Senior Fellowship to DS (WT100986/Z/13/Z), a Vice-Chancellor's Fellowship from the University of Sheffield to AF and a BBSRC project grant (BB/R016925/1).

Author Contributions

D.S. conceived and performed experiments, interpreted results, provided expertise and feedback. K.F. designed and wrote the code, ran simulations and interpreted results. A.F. wrote the code, interpreted results and provided expertise and feedback. All authors wrote and edited the manuscript and secured funding.

Declaration of interests

The authors declare no competing interests.

References

Abley, K., De Reuille, P. B., Strutt, D., Bangham, A., Prusinkiewicz, P., Maree, A. F., Grieneisen, V. A. & Coen, E. (2013). An intracellular partitioning-based framework for tissue cell polarity in plants and animals. Development*, 140*, 2061-74.

Amonlirdviman, K., Khare, N. A., Tree, D. R., Chen, W. S., Axelrod, J. D. & Tomlin, C. J. (2005). Mathematical modeling of planar cell polarity to understand domineering nonautonomy. Science*, 307*, 423-6.

Aw, W. Y. & Devenport, D. (2017). Planar cell polarity: global inputs establishing cellular asymmetry. Curr Opin Cell Biol*, 44*, 110-116.

Axelrod, J. D. (2001). Unipolar membrane association of Dishevelled mediates Frizzled planar cell polarity signaling. Genes Dev*, 15*, 1182-7.

Bastock, R. & Strutt, D. (2007). The planar polarity pathway promotes coordinated cell migration during Drosophila oogenesis. Development*, 134*, 3055-64.

Bastock, R., Strutt, H. & Strutt, D. (2003). Strabismus is asymmetrically localised and binds to Prickle and Dishevelled during *Drosophila* planar polarity patterning. Development*, 130*, 3007-14.

Burak, Y. & Shraiman, B. I. (2009). Order and stochastic dynamics in *Drosophila* planar cell polarity. PLoS Comput Biol*, 5*, e1000628.

Butler, M. T. & Wallingford, J. B. (2017). Planar cell polarity in development and disease. Nat Rev Mol Cell Biol*, 18*, 375-388.

Chae, J., Kim, M. J., Goo, J. H., Collier, S., Gubb, D., Charlton, J., Adler, P. N. & Park, W. J. (1999). The *Drosophila* tissue polarity gene *starry night* encodes a member of the protocadherin family. Development*, 126*, 5421-9.

Chen, W. S., Antic, D., Matis, M., Logan, C. Y., Povelones, M., Anderson, G. A., Nusse, R. & Axelrod, J. D. (2008). Asymmetric homotypic interactions of the atypical cadherin Flamingo mediate intercellular polarity signaling. Cell*, 133*, 1093-105.

Cho, B., Pierre-Louis, G., Sagner, A., Eaton, S. & Axelrod, J. D. (2015). Clustering and negative feedback by endocytosis in planar cell polarity signaling is modulated by ubiquitinylation of Prickle. PLoS Genet*, 11*, e1005259.

Davey, C. F. & Moens, C. B. (2017). Planar cell polarity in moving cells: think globally, act locally. Development*, 144*, 187-200.

Devenport, D. (2014). The cell biology of planar cell polarity. J Cell Biol*, 207*, 171-9.

Emery, G., Hutterer, A., Berdnik, D., Mayer, B., Wirtz-Peitz, F., Gaitan, M. G. & Knoblich, J. A. (2005). Asymmetric Rab 11 endosomes regulate delta recycling and specify cell fate in the *Drosophila* nervous system. Cell*, 122*, 763-73.

Feiguin, F., Hannus, M., Mlodzik, M. & Eaton, S. (2001). The ankyrin repeat protein Diego mediates Frizzled-dependent planar polarization. Dev Cell*, 1*, 93-101.

Fischer, S., Houston, P., Monk, N. A. & Owen, M. R. (2013). Is a persistent global bias necessary for the establishment of planar cell polarity? PLoS One*, 8*, e60064.

Goodrich, L. V. & Strutt, D. (2011). Principles of planar polarity in animal development. Development*, 138*, 1877-1892.

Gubb, D. & Garcia-Bellido, A. (1982). A genetic analysis of the determination of cuticular polarity during development in *Drosophila melanogaster*. J Embryol Exp Morphol*, 68*, 37-57.

Gubb, D., Green, C., Huen, D., Coulson, D., Johnson, G., Tree, D., Collier, S. & Roote, J. (1999). The balance between isoforms of the Prickle LIM domain protein is critical for planar polarity in *Drosophila* imaginal discs. Genes Dev*, 13*, 2315-27.

Jenny, A., Reynolds-Kenneally, J., Das, G., Burnett, M. & Mlodzik, M. (2005). Diego and Prickle regulate Frizzled planar cell polarity signalling by competing for Dishevelled binding. Nat Cell Biol*, 7*, 691-697.

Jones, K. H., Liu, J. & Adler, P. N. (1996). Molecular analysis of EMS-induced *frizzled* mutations in *Drosophila melanogaster*. Genetics*, 142*, 205-15.

Klein, T. J. & Mlodzik, M. (2005). Planar Cell Polarization: An Emerging Model Points in the Right Direction. Annu Rev Cell Dev Biol*, 21*, 155-176.

Klünder, B., Freisinger, T., Wedlich-Söldner, R. & Frey, E. (2013). GDI-mediated cell polarization in yeast provides precise spatial and temporal control of Cdc42 signaling. PLoS Comput Biol*, 9*, e1003396.

Lawrence, P. A., Casal, J. & Struhl, G. (2004). Cell interactions and planar polarity in the abdominal epidermis of *Drosophila*. Development*, 131*, 4651-4664.
Le Garrec, J. F., Lopez, P. & Kerszberg, M. (2006). Establishment and maintenance of planar epithelial cell polarity by asymmetric cadherin bridges: a computer model. Dev Dyn*, 235*, 235-246.
Lee, T. & Luo, L. (1999). Mosaic analysis with a repressible cell marker for studies of gene function in neuronal morphogenesis. Neuron*, 22*, 451-61.
Locke, M. (1959). The Cuticular Pattern in an Insect, Rhodnius-Prolixus Stal. Journal of Experimental Biology*, 36*, 459-476.
Ma, D., Yang, C. H., Mcneill, H., Simon, M. A. & Axelrod, J. D. (2003). Fidelity in planar cell polarity signalling. Nature*, 421*, 543-547.
Piepho, H. (1955). Über die Ausrichtung der Schuppenbälge und Schuppen am Schmetterlingsrumpf. Naturwissenschaften*, 42*, 22-22.
Schamberg, S., Houston, P., Monk, N. A. & Owen, M. R. (2010). Modelling and analysis of planar cell polarity. Bull Math Biol*, 72*, 645-80.
Struhl, G., Casal, J. & Lawrence, P. A. (2012). Dissecting the molecular bridges that mediate the function of Frizzled in planar cell polarity. Development*, 139*, 3665-74.
Strutt, D. (2009). Gradients and the specification of planar polarity in the insect cuticle. Cold Spring Harb Perspect Biol*, 1*, a000489.
Strutt, D. & Strutt, H. (2007). Differential activities of the core planar polarity proteins during *Drosophila* wing patterning. Dev Biol*, 302*, 181-194.
Strutt, D. I. (2001). Asymmetric localization of Frizzled and the establishment of cell polarity in the *Drosophila* wing. Mol Cell*, 7*, 367-75.
Strutt, H., Gamage, J. & Strutt, D. (2016). Robust Asymmetric Localization of Planar Polarity Proteins Is Associated with Organization into Signalosome-like Domains of Variable Stoichiometry. Cell Rep*, 17*, 2660-2671.
Strutt, H. & Strutt, D. (2008). Differential stability of Flamingo protein complexes underlies the establishment of planar polarity. Curr Biol*, 18*, 1555-1564.
Strutt, H. & Strutt, D. (2009). Asymmetric localisation of planar polarity proteins: Mechanisms and consequences. Semin Cell Dev Biol*, 20*, 957-63.
Strutt, H., Warrington, S. J. & Strutt, D. (2011). Dynamics of core planar polarity protein turnover and stable assembly into discrete membrane subdomains. Dev Cell*, 20*, 511-525.
Taylor, J., Abramova, N., Charlton, J. & Adler, P. N. (1998). *Van Gogh*: a new *Drosophila* tissue polarity gene. Genetics*, 150*, 199-210.
Theisen, H., Purcell, J., Bennett, M., Kansagara, D., Syed, A. & Marsh, J. L. (1994). *dishevelled* is required during *wingless* signaling to establish both cell polarity and cell identity. Development*, 120*, 347-60.
Tree, D. R., Shulman, J. M., Rousset, R., Scott, M. P., Gubb, D. & Axelrod, J. D. (2002). Prickle mediates feedback amplification to generate asymmetric planar cell polarity signaling. Cell*, 109*, 371-81.
Usui, T., Shima, Y., Shimada, Y., Hirano, S., Burgess, R. W., Schwarz, T. L., Takeichi, M. & Uemura, T. (1999). Flamingo, a seven-pass transmembrane cadherin, regulates planar cell polarity under the control of Frizzled. Cell*, 98*, 585-95.
Vinson, C. R. & Adler, P. N. (1987). Directional non-cell autonomy and the transmission of polarity information by the *frizzled* gene of *Drosophila*. Nature*, 329*, 549-551.
Warrington, S. J., Strutt, H., Fisher, K. H. & Strutt, D. (2017). A Dual Function for Prickle in Regulating Frizzled Stability during Feedback-Dependent Amplification of Planar Polarity. Curr Biol*, 27*, 2784 - 2797.e3.
Wu, J. & Mlodzik, M. (2008). The Frizzled extracellular domain is a ligand for Van Gogh/Stbm during nonautonomous planar cell polarity signaling. Dev Cell*, 15*, 462-9.

Figure 1

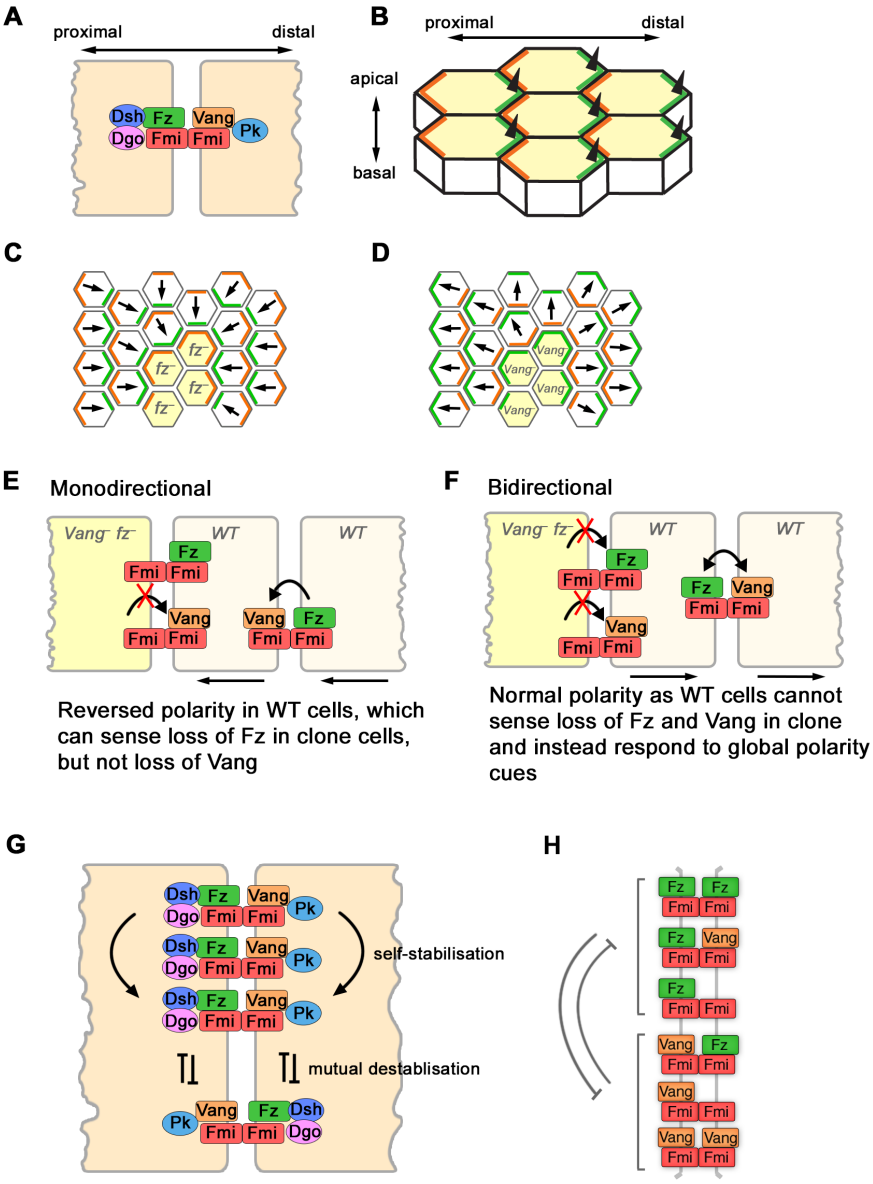

Figure 1. Directional signalling in planar polarity.

(A) Diagram of the core planar polarity proteins localising to form an intercellular complex at a junction between two cells.

(B) Diagram showing asymmetric localisation of Fz (green) and Vang (orange) in the developing *Drosophila* wing. Black triangles represent trichomes emerging at distal cell ends of the apical wing surface.

(C,D) Diagrams of non-autonomous phenotypes of *fz*⁻ (C) and *Vang*⁻ (D) clones (yellow cells) in pupal wings. Arrows represent trichome orientation. At the edge of a *fz*⁻ clone, Vang within the clone cells localises to the boundary with wild-type neighbours, indicating it preferentially forms asymmetric complexes with Fz at cell-cell contacts. Similarly, Fz localises at the boundary of *Vang*⁻ clones.

(E,F) Monodirectional (E) and bidirectional (F) signalling predictions. In monodirectional signalling (E), Vang acts as a ligand for Fz and can 'sense' its levels in neighbouring wild-type (WT) cells. *Vang*$^{-}$ *fz*$^{-}$ clones behave identically to *fz*$^{-}$ clones, since no information on Vang levels is transmitted between cells. Cells distal to the clone have reversed polarity (black arrows). In bidirectional signalling (F), no information can be passed from *Vang*$^{-}$ *fz*$^{-}$ cells since both are required for sending and receiving the signal. Thus neighbouring wild-type cells are blind to the clone and polarise normally (black arrows).

(G) Diagram of possible feedback interactions. Stabilising interactions occur locally between complexes of 'like' orientations, whereas destabilising interactions occur between complexes of 'unlike' orientations.

(H) Diagram of destabilising feedbacks simulated between different possible Fz- and Vang-containing complexes localised at a junction between two cells in our computational modelling framework.

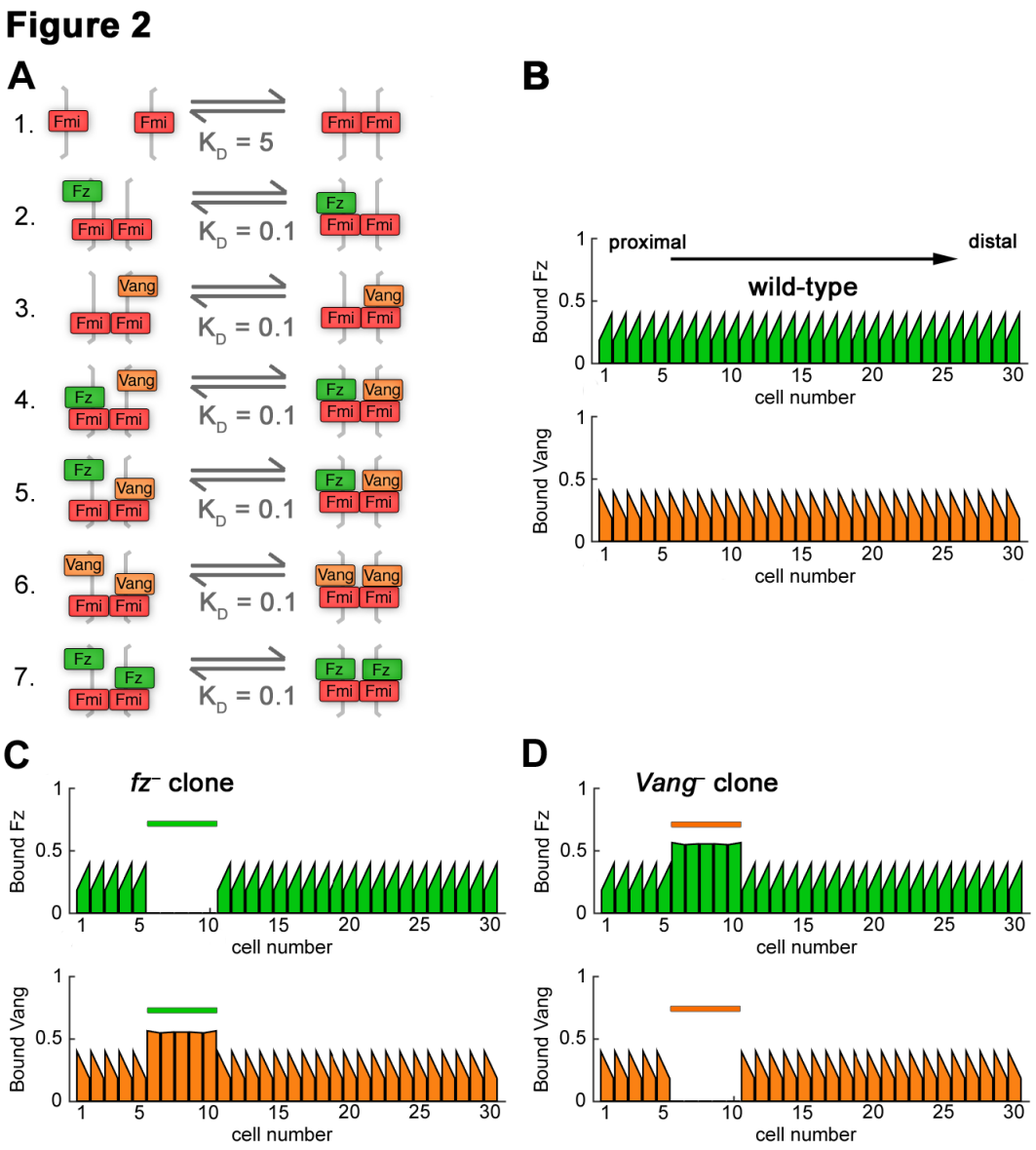

Figure 2. Polarity is generated in simulations with no direct signalling.

(A) Model 1 biochemical binding reactions with relative dissociation constants K_D. Higher K_D corresponds to weaker binding.

(B) Simulation of wild-type polarity at steady state showing amount of bound Fz (top) and bound Vang (bottom) on the proximal and distal sides of each cell. Bound Fz levels (i.e. sum of complexes that contain Fz within each compartment; upper panels, green graphs) and bound Vang levels (lower panels, orange graphs) are shown for each cell edge.

(C,D) Simulation at steady state ($V_{max,F}$ = $V_{max,V}$ = 10) for *fz*⁻ (C) or *Vang*⁻ (D) clones. Sloped tops of bars indicate the cell is polarised for that protein. Coloured bars above graphs indicate clone cells (in cell numbers 6-10). Cells neighbouring the clones show normal polarity and thus clones are autonomous.

Figure 3

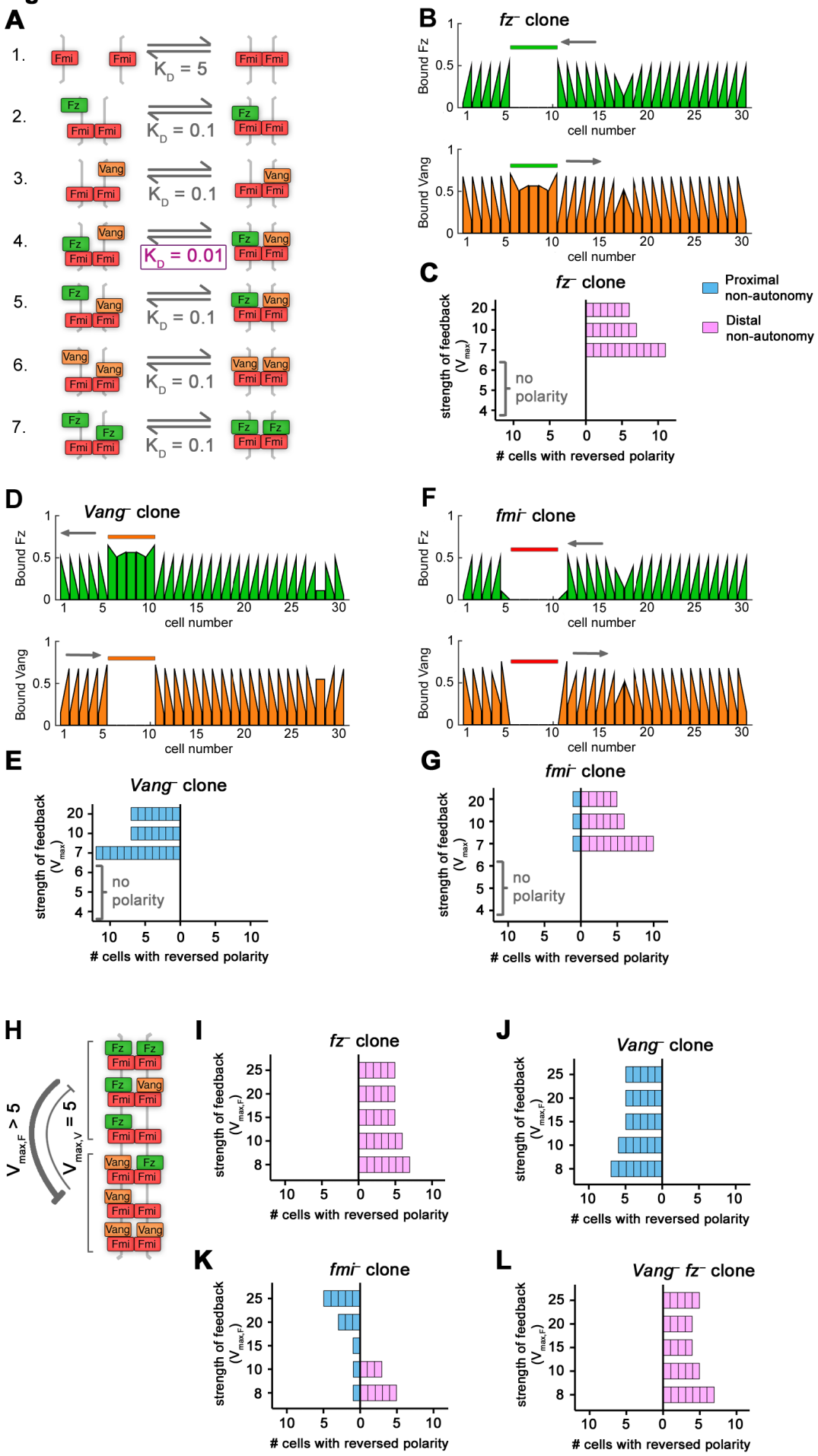
A
1.
2.
3.
4.
5.
6.
7.
Fz
Vang
Fmi
K_D = 5
K_D = 0.1
K_D = 0.01
B
fz⁻ clone
Bound Fz
Bound Vang
cell number
C
fz⁻ clone
Proximal non-autonomy
Distal non-autonomy
strength of feedback (V_{max})
no polarity
cells with reversed polarity
D
Vang⁻ clone
E
Vang⁻ clone
F
fmi⁻ clone
G
fmi⁻ clone
H
$V_{max,F}$ > 5
$V_{max,V}$ = 5
I
fz⁻ clone
strength of feedback ($V_{max,F}$)
J
Vang⁻ clone
K
fmi⁻ clone
L
Vang⁻ fz⁻ clone

Figure 3. Direct monodirectional signalling can reproduce *in vivo* clone phenotypes

(A) Model 2 biochemical binding reactions with relative dissociation constants, K_D, for direct monodirectional signalling. In this model, Vang is better at binding (i.e. has a lower dissociation constant) to complexes that already have Fz bound in the neighbouring cell (reaction 4) compared to other complexes (reactions 3 and 6). This allows Vang to receive a 'signal' from Fz.

(B,D,F) Bound Fz levels (upper panels, green graphs) and bound Vang levels (lower panels, orange graphs) at each cell edge from simulations, with equal feedback strengths ($V_{max,F} = V_{max,V} = 10$), at steady state for *fz*⁻ (B), *Vang*⁻ (D) or *fmi*⁻ (F) clones. Sloped tops of bars indicate the cell is polarised for that protein. Coloured bars above graphs indicate clone cells (in cell numbers 6-10). Grey arrows indicate regions of non-autonomous polarity.

(C,E,G) Non-autonomy around clones from simulations at steady state with varying, but balanced, feedback strength (where V_{max} represents $V_{max,F} = V_{max,V}$). Results shown for *fz*⁻ (C), *Vang*⁻ (E), or *fmi*⁻ (G) clones. Parameter conditions where no polarity was observed in the absence of clones are indicated ('no polarity').

(H) Diagram indicating unbalanced feedback interaction strengths with stronger feedback from Fz as compared to Vang ($V_{max,F} > V_{max,V}$).

(I-L) Simulations of monodirectional signalling with unbalanced feedback strengths as in (H), where $V_{max,V} = 5$ and $V_{max,F} > 5$, show distal and proximal non-autonomy around *fz*⁻ (I) and *Vang*⁻ (J) clones, respectively. However, *fmi*⁻ clones (K) show non-autonomy varying from distal to proximal as $V_{max,F}$ increases, while *Vang*⁻ *fz*⁻ double clones (L) show distal non-autonomy for all parameters shown. If $V_{max,V} = 5$, *fmi*⁻ clones show no non-autonomy only in the case $V_{max,F} = 15$; in this case, double clones show distal non-autonomy.

Figure 4

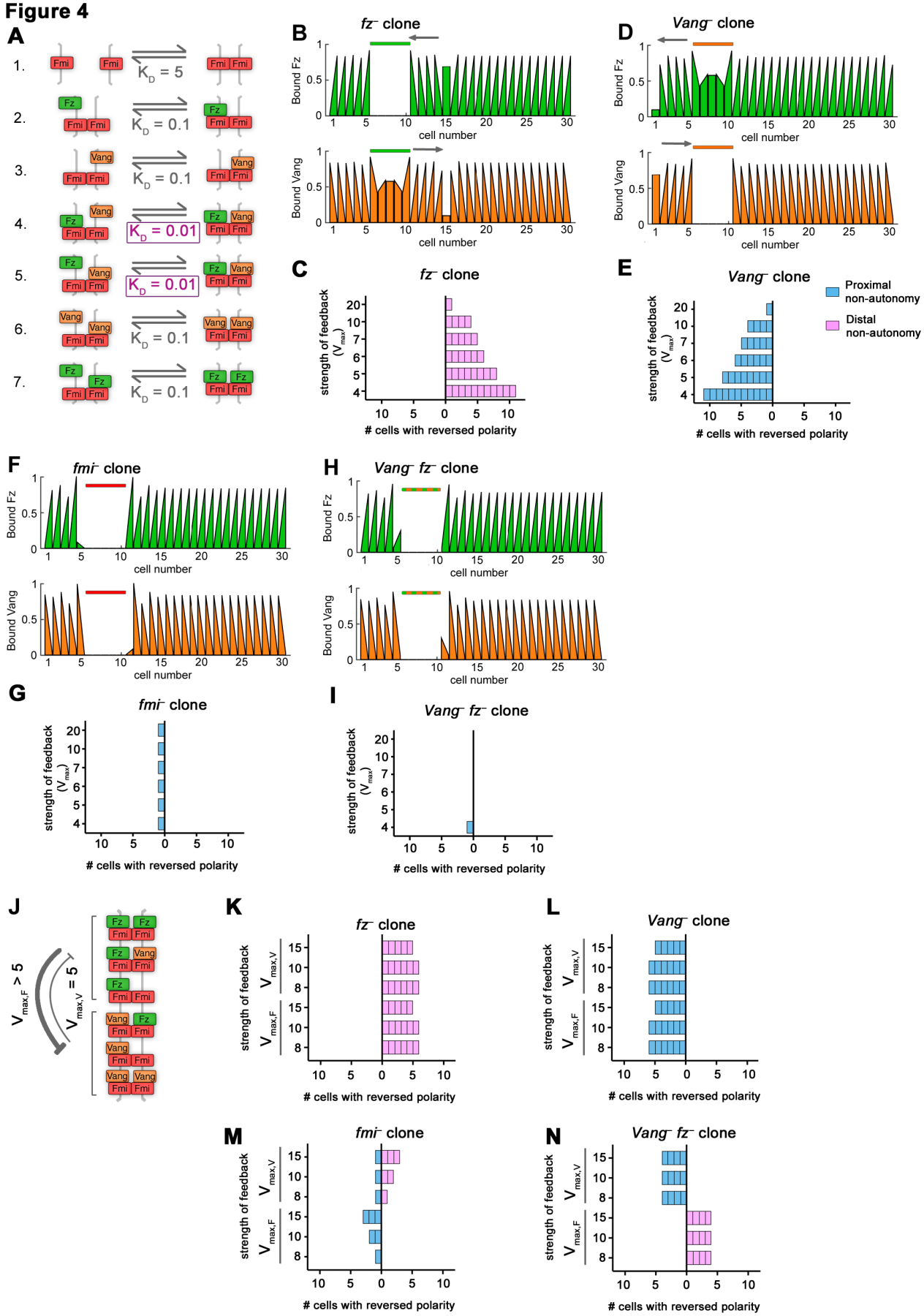
A
1.
2.
3.
4.
5.
6.
7.
Fmi
Fz
Vang
K_D = 5
K_D = 0.1
K_D = 0.01
B
fz⁻ clone
Bound Fz
Bound Vang
cell number
C
fz⁻ clone
strength of feedback (V_{max})
cells with reversed polarity
D
Vang⁻ clone
E
Vang⁻ clone
Proximal non-autonomy
Distal non-autonomy
F
fmi⁻ clone
G
fmi⁻ clone
H
Vang⁻ fz⁻ clone
I
Vang⁻ fz⁻ clone
J
$V_{max,F}$ > 5
$V_{max,V}$ = 5
K
fz⁻ clone
L
Vang⁻ clone
M
fmi⁻ clone
N
Vang⁻ fz⁻ clone
$V_{max,V}$
$V_{max,F}$

Figure 4. Direct bidirectional signalling reproduces *in vivo* clone phenotypes

(A) Model 3 biochemical binding reactions with relative Dissociation Constants, K_D, for direct bidirectional signalling. In this model, Vang is better at binding (i.e. has a lower dissociation constant) to complexes that already have Fz bound in the neighbouring cell (reaction 4) compared to other complexes (reactions 3 and 6) and Fz is *also* better at binding when Vang is present in the complex (reaction 5 compared to 2 and 7). This allows both Vang and Fz to receive information in the form of mass action binding kinetics.

(B,D,F,H) Bound Fz levels (upper panels, green graphs) and bound Vang levels (lower panels, orange graphs) at each cell edge from simulations at steady state for one parameter set ($V_{max,F}$ = $V_{max,V}$ = 10) for *fz*$^-$ (B), *Vang*$^-$ (D), *fmi*$^-$ (F), or *Vang*$^-$ *fz*$^-$ (H) clones. Coloured bars above graphs indicate clone cells (in cell numbers 6-10). Grey arrows indicate regions of non-autonomous polarity.

(C,E,G,I) Non-autonomy around clones from simulations at steady state with varying, but balanced, feedback strength (where V_{max} represents $V_{max,F}$ = $V_{max,V}$). Results shown for *fz*$^-$ (C), *Vang*$^-$ (E), *fmi*$^-$ (G), or *Vang*$^-$ *fz*$^-$ (I) clones.

(J) Diagram showing an example of unbalanced intracellular destabilising feedbacks between Fz and Vang. In this example there is stronger feedback from Fz than from Vang.

(K-N) Non-autonomy around clones from simulations at steady state with unbalanced feedback strength for *fz*$^-$ (K), *Vang*$^-$ (L), *fmi*$^-$ (M), or *Vang*$^-$ *fz*$^-$(N). For the top half of each graph $V_{max,V}$ is >5 as indicated and $V_{max,F}$ = 5. For the lower bars of each graph, $V_{max,F}$ is > 5 as indicated and $V_{max,V}$ = 5. Clones of *fz*$^-$ and *Vang*$^-$ show distal and proximal non-autonomy, respectively. However, *fmi*$^-$ clones show distal non-autonomy when $V_{max,F}$ is higher, but proximal non-autonomy when $V_{max,V}$ is higher. The direction of non-autonomy is reversed for *Vang*$^-$ *fz*$^-$ double clones, showing distal non-autonomy when $V_{max,V}$ is higher, but proximal non-autonomy when $V_{max,F}$ is higher.

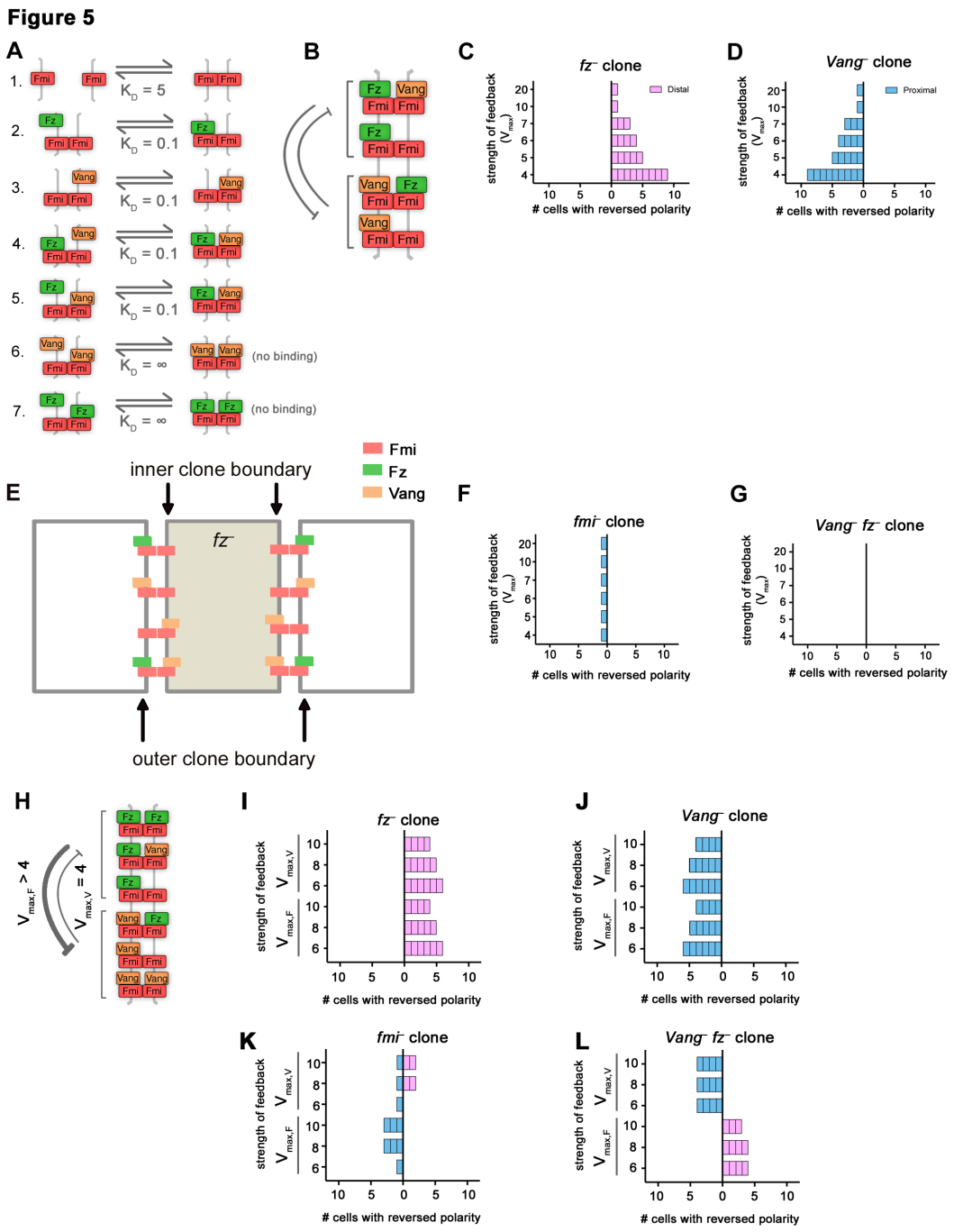

Figure 5. In the absence of symmetric complexes feedback interactions determine directionality of indirect signalling

(A) Model 4 biochemical binding reactions with relative dissociation constants K_D. Symmetric complexes in reactions 6 and 7 do not form.

(B) Diagram showing bidirectional intracellular destabilising feedbacks between Fz and Vang implemented in this model.

(C,D,F,G) Non-autonomy around clones from simulations at steady state for *fz*⁻ (C), *Vang*⁻ (D), *fmi*⁻ (F), or *Vang*⁻ *fz*⁻ (G). Feedback strength varies as indicated (where $V_{max} = V_{max,F} = V_{max,V}$).

(E) Diagram of complex formation with ‘no direct signalling’ in the absence of symmetric complexes at the boundary of a *fz*$^{-}$ clone. There are more possibilities for Fz than Vang to bind at the outer clone boundaries, which generates distal non-autonomy.

(H) Diagram showing an example of unbalanced intracellular destabilising feedbacks between Fz and Vang. In this case there is stronger feedback from Fz than from Vang.

(I-L) Non-autonomy around clones from simulations at steady state with unbalanced feedback strength for *fz*$^{-}$ (I), *Vang*$^{-}$ (J), *fmi*$^{-}$ (K), or *Vang*$^{-}$ *fz*$^{-}$ (L). For the top half of each graph $V_{max,\mathrm{V}}$ is indicated as >4 and $V_{max,\mathrm{F}}$ = 4. For the lower bars of each graph, $V_{max,\mathrm{F}}$ is indicated as >4 and $V_{max,\mathrm{V}}$ = 4.

Figure 6

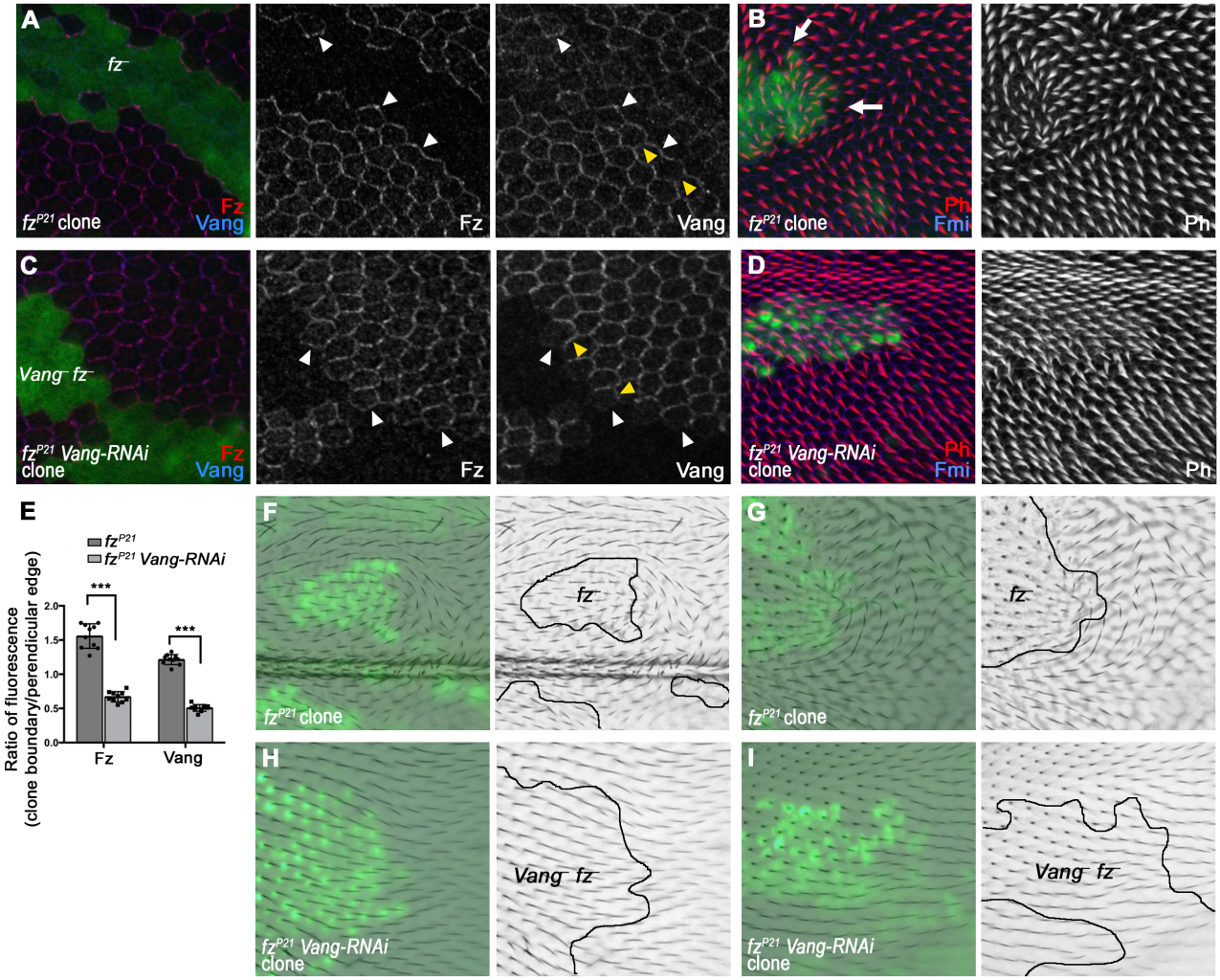

Figure 6. Non-autonomy around *fz*⁻ clones is suppressed by simultaneous knockdown of *Vang* activity by RNAi.

(A-D) Pupal wings with loss-of-function MARCM clones of fz^{P21} alone (A,B), or fz^{P21} clones also expressing *UAS-Vang-RNAi* . Wings were immunolabelled for Fz (red) and Vang (blue) at 28 h after pupa formation (APF; A,C), or for Phalloidin to mark trichomes (red) and Fmi (blue) at 32.25 h APF (B,D). White arrowheads point to clone boundaries and yellow arrowheads point to cell edges perpendicular to the clone boundary. White arrows show areas of reversed trichome polarity. GFP (green) positively marks the clones. Representative images from at least 9 clones per genotype are shown.

(E) Ratio of Fz and Vang fluorescence intensities at clone boundaries (white arrowheads in A and C) and perpendicular edges (yellow arrowheads in A and C). For *fz*⁻ clones (dark grey bars), Fz and Vang are recruited to the clone boundaries and so ratio values are above 1. However, for *Vang*⁻ *fz*⁻ clones (light grey bars), Fz and Vang do not accumulate at the boundary and thus ratio values are below 1. Measurements were taken from 10 wings per genotype (n = 10), averaged from at least 7 regions of each type per wing. Two-way ANOVA was employed with Sidak's multiple comparison test, *** $p < 0.0001$.

(F-I) Adult wings with clones of *fz*^{P21} (F,G) or *fz*^{P21} *UAS-Vang-RNAi* (H,I). Green nuclei mark clone cells and brightfield images show trichomes. Two representative examples from at least 10 clones are shown for each genotype. All panels are aligned with proximal left and anterior up.

Table 1. Summary of planar polarity models.

						Reproduces clone phenotypes?			
Complex formation	**Direct signalling (via differential K_D of complexes)**	**Model number**	**Feedback interactions**	**Figure**	**polarises?**	***fz***	***Vang***	***fmi***	**Prediction for *Vang fz* clones**
Includes symmetric complexes	none	1	Fz on Vang and Vang on Fz ($V_{max,V} = V_{max,F}$ balanced strengths)	Figure 2	yes	no	no	-	-
			Fz on Vang and Vang on Fz ($V_{max,V} > V_{max,F}$ or $V_{max,F} > V_{max,V}$ unbalanced)	Figure S2	no	-	-	-	-
	monodirectional	2	Fz on Vang and Vang on Fz ($V_{max,V} = V_{max,F}$ balanced strengths)	Figure 3	yes	yes	yes	no	-
			Fz on Vang and Vang on Fz ($V_{max,V} > V_{max,F}$)	-	no	-	-	-	-
			Fz on Vang and Vang on Fz ($V_{max,F} = 15$, $V_{max,V} = 5$)	Figure 3	yes	yes	yes	yes	distal non-autonomy
	bidirectional	3	Fz on Vang and Vang on Fz ($V_{max,V} = V_{max,F}$ balanced strengths)	Figure 4	yes	yes	yes	yes	no non-autonomy
			Fz on Vang and Vang on Fz ($V_{max,V} > V_{max,F}$ weakly unbalanced)	Figure 4	yes	yes	yes	yes	proximal non-autonomy
			Fz on Vang and Vang on Fz ($V_{max,V} \gg V_{max,F}$ strongly unbalanced)	Figure 4	yes	yes	yes	no	-
			Fz on Vang and Vang on Fz ($V_{max,F} > V_{max,V}$ weakly unbalanced)	Figure 4	yes	yes	yes	yes	distal non-autonomy
			Fz on Vang and Vang on Fz ($V_{max,F} \gg V_{max,V}$ strongly unbalanced)	Figure 4	yes	yes	yes	no	-
No symmetric complexes	none	4	Fz on Vang and Vang on Fz ($V_{max,V} = V_{max,F}$ balanced strengths)	Figure 5	yes	yes	yes	yes	no non-autonomy
			Fz on Vang and Vang on Fz ($V_{max,V} > V_{max,F}$ weakly unbalanced)	Figure 5	yes	yes	yes	yes	proximal non-autonomy
			Fz on Vang and Vang on Fz ($V_{max,V} \gg V_{max,F}$ strongly unbalanced)	Figure 5	yes	yes	yes	no	-
			Fz on Vang and Vang on Fz ($V_{max,F} > V_{max,V}$ weakly unbalanced)	Figure 5	yes	yes	yes	yes	distal non-autonomy
			Fz on Vang and Vang on Fz ($V_{max,F} \gg V_{max,V}$ strongly unbalanced)	Figure 5	yes	yes	yes	no	-